Conformation of Polymer Brushes at Aqueous Surfaces Determined with X-ray and Neutron Reflectometry. 2. High-Density Phase Transition of Lipopolyoxazolines

A. Wurlitzer,[†] E. Politsch,[‡] S. Huebner,[‡] P. Krüger,[†] M. Weygand,[†] K. Kjaer,[§] P. Hommes,[⊥] O. Nuyken,[⊥] G. Cevc,[‡] and M. Lösche*,[†]

Institute of Experimental Physics I, University of Leipzig, Linnéstr. 5, D-04103 Leipzig, Germany; Institute of Medical Biophysics, Technical University of Munich, Ismaninger Str. 22, D-81675 München, Germany; Department of Condensed Matter Physics and Chemistry, Risø National Laboratory, DK-4000 Roskilde, Denmark; and Institute of Technical Chemistry, Technical University of Munich, D-85747 München, Germany

Received May 26, 2000

ABSTRACT: We have investigated the molecular conformations of a lipopolymer with a polyoxazoline headgroup at air/water interfaces as a function of lateral area per molecule with X-ray and neutron reflectometry. The polymer 1,2-dioctadecanyl-*sn*-glycero-3-poly(2-methyl-2-oxazoline), PMO−$(C_{18})_2$, forms stable surface monolayers. Pressure/area isotherms around room temperature show a plateau region, indicative of a phase transition whose origin was examined. For data evaluation, a novel approach was used that acts on explicit quasi-molecular ensemble conformations of the polymer [Politsch et al., preceding paper in this issue]. At lower surface pressure, the polymer density distribution exhibits a maximum near the interface, indicative of attractive interaction between the predominantly hydrophilic polymer chains and the hydrophobic surface. Across the plateau region of the isotherm, a change in the volume density distribution of the alkyl chains was observed which is indicative of a partial immersion of the lipid moieties into the aqueous subphase. In contrast, no major structural change across the phase transition was detected in the polymer volume density profiles which comply with scaling predictions at both sides of the phase transition if deviations due to nonidealities are neglected. We interpret these observations as an alkyl chain ordering induced by the steric interference between the PMO: Immersion of alkyl chains into the subphase relaxes the strain on the hydrophobic anchors which derives from a reduction of the configurational entropy of the PMO chains due to their confinement to the interface.

1. Introduction

Lipopolymers consist of hydrophilic polymers covalently attached to the polar headgroups of amphiphilic molecules. Through their hydrophobic tails such amphiphiles may be anchored to interfaces that divide a hydrophilic from a hydrophobic compartment, such as an aqueous surface or the interface of a lipid membrane with water. Equilibrium conformations and forces in the resulting "tethered" polymer layers have received considerable attention in recent years owing to a wide range of potential applications, such as the stabilization of colloidal particles, control of adhesion, and the biocompatibilization of interfaces. In particular, attention has been paid to the employment of lipopolymers for the purpose of drug carriers:[1] Sterically stabilized vesicles may be prepared by an admixture of small amounts of lipopolymers to physiological lipids in membranes. Vesicles masked in such a way circulate considerably longer in the bloodstream.[2,3] Lipopolymers also serve as model system to test theories describing grafted polymers at interfaces.[4−6]

The most thoroughly investigated lipopolymers to date are poly(ethylene glycol) (PEG) lipids.[5,7,8] However, several more lipopolymers have been described that vary in size and functionality.[4,5,9]

Recently, a novel method has been developed to synthesize lipopolymers with polyoxazoline headgroups.[10] In the so-called "initiator method", a suitably substituted hydrophobic group (e.g., a lipid) initiates the living polymerization of cyclic iminoethers (oxazolines). This technique allows selective synthesis of a whole family of oxazoline lipopolymers, varying in molecular weight and functionality, and facilitates the design of complex structures that may be adapted to potential application requirements. A relatively simple and promising derivative is PMO−$(C_{18})_2$ in which a poly(methyloxazoline) group is attached to the glycerol backbone of an ether lipid (cf. Figure 1). Vesicles sterically stabilized with PMO−$(C_{18})_2$ circulate longer in the bloodstream, as do PEG lipids, in comparison with conventional liposomes without such polymers.[10]

To obtain insight into the conformational behavior of PMO−$(C_{18})_2$, we have initiated investigations at the air/water interface in which the area per molecule, A, was well controlled. PMO−$(C_{18})_2$ forms stable monolayers at lateral pressures up to $\pi \sim 40$ mN/m. The corresponding room temperature $\pi-A$ isotherm shows a plateau region at $\pi \sim 25$ mN/m and $A \sim 150$ Å^2. Conceptually, such a plateau may be caused by a first-order phase transition, either a mushroom-to-brush transition[11,12] within the polymer or a condensation of the lipid hydrocarbon chains.[13] In practical terms, a mushroom-to-brush transition is expected at $A \sim 900$ Å^2 for the PMO−$(C_{18})_2$ species studied here. On the

[†] University of Leipzig.
[‡] Institute of Medical Biophysics, Technical University of Munich.
[§] Risø National Laboratory.
[⊥] Institute of Technical Chemistry, Technical University of Munich.
* Corresponding author. Phone +49 (341) 97-32 488; fax +49 (341) 97-32 470; e-mail loesche@physik.uni-leipzig.de.

10.1021/ma000932n CCC: $20.00
Published on Web 01/30/2001

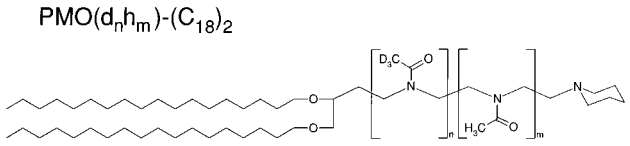

Figure 1. Chemical structure of the lipopolyoxazoline.

other hand, chain condensation driven by van der Waals interactions between alkyl chains of conventional phospholipids are typically observed at $A < 70$ Å^2.[14] To elucidate the origin of the phase transition in PMO−$(C_{18})_2$ monolayers, studies by infrared reflection−absorption spectroscopy (IRRAS) have been performed:[6,13] A bathochromic frequency shift of the symmetric and asymmetric methylene stretching modes has been observed across the plateau, indicating a significant increase in the molecular order of the CH_2 groups on the lipopolymer. For a different type of lipopolymers, PEG lipids, which show a similar plateau region, it has been recently shown by comparison of species with fully deuterated and fully hydrogenated lipid alkyl chains that this change must be attributed to the alkyl chains.[15] However, IRRAS cannot resolve the origin of this ordering process that is observed at molecular areas which turn out to be unusually large if compared with areas where chain condensation occurs in conventional (phospho)lipids. Initial neutron and X-ray reflectivity measurements have supplied a relatively coarse assessment of the PMO−$(C_{18})_2$ organization at the interface[16] with no evidence for a conformational change of the polymer chains across the plateau region. The investigations presented here provide a more detailed picture of the molecular density distribution across the interface and thus yield deeper insight into the changes of molecular conformation as a function of area density, which allows a more rigorous interpretation.

2. Materials and Methods: Theoretical Predictions

Materials and Experimental Design. The synthesis of the lipopolymer 1,2-dioctadecanyl-*sn*-glycero-3-poly(2-methyl-2-oxazoline), PMO−$(C_{18})_2$ (Figure 1), has been described in the literature.[10] We investigated one PMO species with a specific deuteration pattern, PMO(d_8h_{30})−$(C_{18})_2$, along its hydrophilic polymer chain. It consists on average of 38 monomer units, of which the eight closest to the alkyl chains are deuterated. The sample is characterized by a polydispersity index of $\langle M_w\rangle/\langle M_n\rangle \sim 1.19$. For use in the experiments, PMO−$(C_{18})_2$ was dissolved in chloroform (p.a., Merck, Darmstadt) and deposited on the subphase by spreading with a microsyringe. Aqueous subphases were prepared using purified water (resistivity $\Omega >$ 18 MΩ·cm, Milli-Q, Millipore, Eschborn/Germany). $\pi-A$ isotherms were measured on subphases whose pH was adjusted by buffering with 0.1 mM KPP (pH = 6.5) or with 25 mM HCl or NaOH (pH = 1.6 or 12.4, respectively). Reflectivity measurements were taken from films prepared on pure water.

The Langmuir troughs used for measurements of the isotherms and of reflectivities of the surface films are of local design. Isotherms were measured on a trough with a symmetric barrier setup and a maximum area of 12 × 20 cm^2. The troughs used in X-ray and neutron reflectivity measurements have a surface area of 16 × 28 cm^2. All troughs are thermostated: The ones used for isotherm and for X-ray measurements use Peltier elements to obtain a thermal stability of ∼0.2 K; the one used in neutron measurements uses thermostated water and has a thermal stability of better than 1 K. Surface pressures were always determined using the Wilhelmy method.[17]

X-ray experiments were performed on a dedicated liquid surface reflectometer (JJ X-ray, Roskilde) located at the University of Leipzig.[18] The radiation source is a sealed Cu anode ($\lambda \sim 1.54$ Å, $U = 45$ kV, $I = 35$ mA) with a line focus (Bruker AXS, Karlsruhe). Its beam is collimated by a graded parabolic multilayer mirror optimized for Cu Kα radiation (Bruker AXS). The intensity of the primary beam at the sample is about 4×10^7 photons/s. Signal and background collection is achieved simultaneously using a position-sensitive detector (Braun, München). With this instrument, X-ray reflectivities above $R \sim 5 \times 10^{-9}$ can be determined.

Neutron reflectivity experiments were performed at the liquid surface reflectometer TAS 9 in the guide hall of the DR3 reactor at Risø National Laboratory.[19] Reflectivity data were obtained at $T \sim 15$ °C using lateral pressures below and above the phase transition ($\pi = 17.5$ and 30 mN/m, respectively) on H_2O and D_2O. To enable a simultaneous evaluation of X-ray and neutron data, X-ray measurements have been performed with the same—partially deuterated—PMO(d_8h_{30})−$(C_{18})_2$ polymer that was also used for neutron measurements. PMO−$(C_{18})_2$ films were stable during reflectivity experiments, which took ∼5 h for X-ray and 12−15 h for neutron measurements.

Data Modeling. For data analysis, two different evaluation approaches were pursued: (i) a strip-function approach and (ii) a novel modeling technique developed specifically for the description of linear polymers that optimizes the configurations of a molecular ensemble at the interface using an evolution strategy (ES).[20] Principles and details of these data inversion method are described in a separate publication,[21] preceding the current paper.

The popular strip-function ("box model") approach[22,23] is simple and straightforward to implement and was expected to provide a *qualitative* picture of the molecular structure of the lipopolymer in terms of the polymer segment density normal to the interface, along the local z axis. However, the limited quality of the available experimental data (low range of accessible momentum transfer, Q_z, in neutron measurements and low contrast in X-ray measurements) permitted the use of only a small number of slabs ("boxes") for the description of lipopolymers at the interface. Moreover, neither a molecular interpretation of the revealed slab structures nor a rigorous cross-correlation of neutron and X-ray data was possible. In the implementation used here, each slab i was parametrized with a thickness d_i and a scattering length density (SLD) ρ_i. To smoothen the artificially sharp transitions between adjacent slabs, i and $i+1$, the step functions Θ describing ideally sharp transitions were blurred into error functions

$$\Theta(z - z_i) \rightarrow \frac{1}{2}\,\mathrm{erf}\left(\frac{z - z_i}{\sqrt{2}\sigma_i}\right) + \frac{1}{2}$$

with the parameters σ_i giving the length scales of the transitions. Optimum parameter values corresponding to the best fits were determined by least-squares minimization. For a cross-correlation of X-ray and neutron results in simultaneous refinements of the data, the inherent length scales in the model were coupled to increase the significance of the results. Neutron data sets were thus fitted together with the corresponding X-ray data sets using a set of parameters satisfying eq 1:

$$\frac{b_{\mathrm{X-ray}}}{b_{\mathrm{neutr}}} = \frac{\sum_{i=1}^{3} d_i \rho_{i,\mathrm{X-ray}}}{\sum_{i=1}^{3} d_i \rho_{i,\mathrm{neutr}}} \qquad (1)$$

$b_{\mathrm{X-ray}}$ and b_{neutr} are the respective scattering lengths of polymer plus water under space-filling conditions, d_i is the thickness, and $\rho_{i,\mathrm{X-ray}}$ and $\rho_{i,\mathrm{neutr}}$ are the SLDs of slab i. Even with these restrictions, the approach resulted in numerous local χ^2 minima with similar quality. A consistent picture, even on the qualitative level, was impossible to derive.

To overcome above-mentioned problems, a new data inversion method was used, which is described in detail in an accompanying paper.[21] Briefly, the PMO−$(C_{18})_2$ monolayer was modeled as an ensemble of linear "quasi-molecules" consisting of different molecular segments—alkane, glycerol, deuterated and hydrogenated PMO. For simplicity, the two hydrophobic chains of PMO−$(C_{18})_2$ have been represented as *one* linear segment located at one end of the molecule. The scattering lengths (per unit length) of these segments were determined from their chemical structure; their volumetric cross sections were either taken from the literature (alkane, 44.2 Å^2)[24] or estimated from the Connolly surface[25] of a molecular model that was MM2 optimized in vacuo (glycerol, 16.0 Å^2; PMO, 25.0 Å^2). The segments were divided into subsegments of uniform length, l_{ss} = 8 Å. In deviation from this general rule, the glycerol fragment consisted of one subfragment of 6 Å length; the alkane chains comprised three subfragments, two with a length of 8 Å and one terminal subfragment with a length of 4.8 Å (total alkane fragment length: 22.8 Å). Similarly, PMO subfragments at the interface to neighboring fragments of the molecule may differ in their length from $l_{ss} = 8$ Å. All segments and subsegments were connected with flexible joints for which one set of angles φ_i suffices to determine the contribution of the molecule to the density distribution along z. Since the algorithm parametrizes the molecular configurations, it enables composition−space refinement[26,27] and may thus be used for the simultaneous fitting of various data sets from isotopically distinct samples or of neutron and X-ray data.

The described parametrization of the monolayer structure supports a parameter space that is (almost) infinitely large. An evolution strategy (ES) has been chosen to screen efficiently for relevant ensemble conformations that are compatible with *all* experimental reflectivity data simultaneously while obeying the constraint of space filling in the subphase compartment.

An ensemble of 40 molecules, which reflects the actual PMO chain length distribution, represents an "individual" in the ES algorithm. The angles $\varphi_{i,k}$ describing the angles between adjacent (sub)segments i and $i + 1$ on molecule k are the main constituents of the genome, which defines the phenotype of an ensemble. Other constituents are the distance, ζ_k, between the hydrophobic/hydrophilic interface in a molecule and the aqueous surface, the average area per molecule, A, and the surface roughness parameter σ, which describes the collective roughening of the interface by capillary waves, similar as in strip-function models.

As in the original ES algorithm,[20,28] data modeling proceeded in three steps with $\mu = 30$ "parents" generating $\lambda = 90$ "offspring" individuals in each generation. In each mutation step, the parameter values on a chromosome were varied within a narrow Gaussian distribution (half-width σ_G) centered at zero, such that the mean deviation between parent and descendant genomes was zero. Crossover was allowed to occur with a small probability. For the resulting lipopolymer conformations, volume filling was determined in horizontal slabs of $\Delta z = 2$ Å thickness, and mutations that lead to overfilling in any of those slabs were rejected whereas in underfilled slabs, void volume was filled with water.

The resulting SLD profiles were determined, and their corresponding (X-ray or neutron) reflectivities were compared with the experimental results using a fitness criterion, $\phi \propto \chi^{-2}$, in which χ^2 is defined in the conventional way as the sum of the square deviations between measured and modeled results. We found that the experimentally determined error bars—based entirely on counting statistics—lead to an underrepresentation of the neutron data sets against the X-ray data sets and have thus artificially reduced the neutron error bars in size at the start of modeling runs. In the second half of the runs, however, the original error bars were reinstalled. With this procedure we avoided solutions that were exclusively compliant with the X-ray data while sacrificing compliance with the neutron data. Typically, between 300 and 1300 generations were used. To smoothen the segment distribution profiles and to estimate the confidence limits of the determined volume distributions, we have averaged 16 independent runs for each data point, thus effectively sampling 640 lipopolymer molecules.

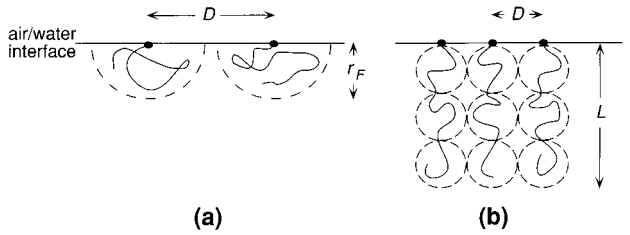

Figure 2. Schematic representation of the "mushroom" (a) and "brush" (b) conformations of surface-grafted polymers.

Scaling Predictions. According to Alexander and de Gennes,[11,12] polymers grafted at interfaces are characterized by (i) the degree of polymerization, N; (ii) the length of a monomer, a; (iii) the layer thickness, L; (iv) the interaction energy of a monomer with the interface, δ (in units of k_BT, $\delta < 0$ for attraction); and (v) the average area per grafted chain, A, and thus the average distance between neighboring chains, $D = A^{1/2}$, and the number density of monomers, $c = N/AL$.

Since water is a good solvent for polyoxazoline, temperature has no effect on polymer conformation and the solvent is considered "athermal". The polymer chains are inscribed in a cubic Flory−Huggins lattice,[29] with a lattice parameter a and a volume per monomer a^3. Each lattice site may be occupied by only one monomer. The average occupation, which is identical to the volume fraction, is Φ.

For grafted polymers, two types of regimes have to be distinguished (Figure 2):[12] At low grafting density, in the "mushroom regime" (Figure 2a), the distance between the grafting points, D, is larger than the Flory radius, $r_F = aN^{3/5}$.[29] Chains then do not overlap. If the density is increased into the "brush" regime (Figure 2b), chains start to interact and are forced to stretch due to mutual repulsion. As first noted by Alexander,[11] the chains can be described as a linear sequence of subunits in this regime, each of size D with a number of monomers g_D:

$$g_D \propto \Phi^{-5/4} = \left(\frac{D}{a}\right)^{5/3} \tag{2}$$

and an overall thickness of the brush, L:

$$L = \frac{ND}{g_D} \propto Na\left(\frac{a}{D}\right)^{2/3} \tag{3}$$

In this regime, the concentration profile is expected to be independent of z,[30] except for two adjustment regions, close to the surface and close to the bulk. Close to the surface, in an interval $a < |z| < D$, the profile is given by

$$\Phi \propto \frac{a^{4/3}z^{2/3}}{D^2} \tag{4}$$

For $D < |z| < L$ the concentration is

$$\Phi \propto \left(\frac{a}{D}\right)^{4/3} \tag{5}$$

and for $|z| > L$, the concentration drops off.

3. Experimental Results

Pressure−Area Isotherms. Figure 3 shows pressure−area (π−A) isotherms of PMO−$(C_{18})_2$ on pure water at different temperatures, T. The general appearance of the isotherms is independent of T: At large areas per molecule, $A > 1500$ Å^2 (not shown), the lateral pressure π starts to increase. At $\pi_p = \pi_p(T)$ and $A_p(T) \sim 190-150$ Å^2, the slopes decrease and the isotherms display a pronounced plateau. At still smaller areas, the

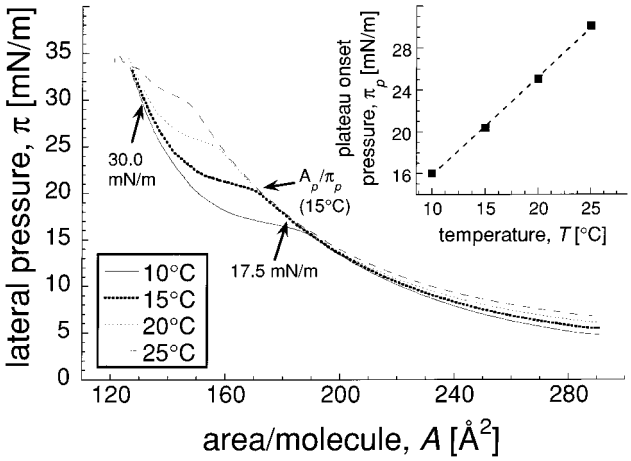

Figure 3. Isotherms of PMO−$(C_{18})_2$ on pure water at various temperatures as indicated. Arrows indicate locations on the isotherm at T = 15 °C, where the X-ray and neutron reflectivities have been measured. Inset: temperature dependence of the plateau onset pressure, π_p.

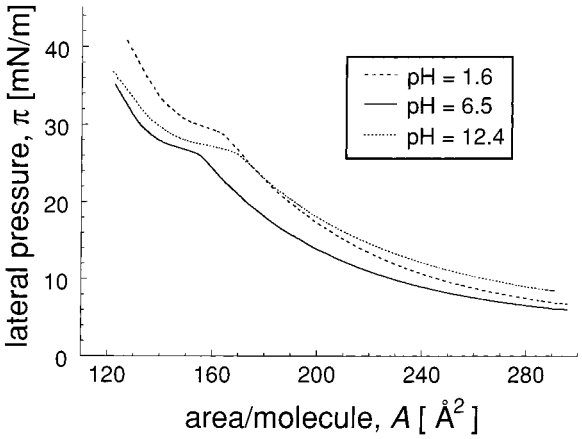

Figure 4. Isotherms (T = 20 °C) of PMO−$(C_{18})_2$ at various pH values of the aqueous subphase as indicated. The subphase at pH = 6.5 has been buffered using 0.1 mM KPP; the other pH values were adjusted by using 25 mM HCl or NaOH.

lateral pressure rises again until the film collapses at $A_c/\pi_c \sim 120$ Å^2 > 35 mN/m. In compression/expansion cycles no hysteresis was observed, indicating that the monolayer is near thermodynamic equilibrium. The plateau onset pressure π_p increases linearly with temperature (cf. inset in Figure 3).

To investigate whether the hydrophilic polymer chains are charged or uncharged in the reflectometry experiments near neutral pH, isotherms have been recorded at various pH values. Amides in aqueous solution are neutral, whereas at low pH protonation takes place since amides are weak bases. With PMO in a basic solution, deprotonation cannot occur since the amide group of the oxazoline is N,N-disubstituted. To verify this, isotherms at pH values between 1.6 and 12.4 are shown in Figure 4. At pH = 6.5, the general appearance of the isotherm was the same as for pH = 12.4, where the molecule is certainly uncharged. The observed shift to higher molecular area A on the basic subphase results from the higher bulk salt concentration; note, however, that the phase transition regime for both pH is in the same π range. At pH = 1.6, where the polymer is protonated, π shifts to significantly higher values and does increasingly so as the area per PMO chain decreases—this includes the phase transition regime. These results give clear indication that PMO is uncharged at pH = 6.5, under conditions where reflectivity measurements have been performed.

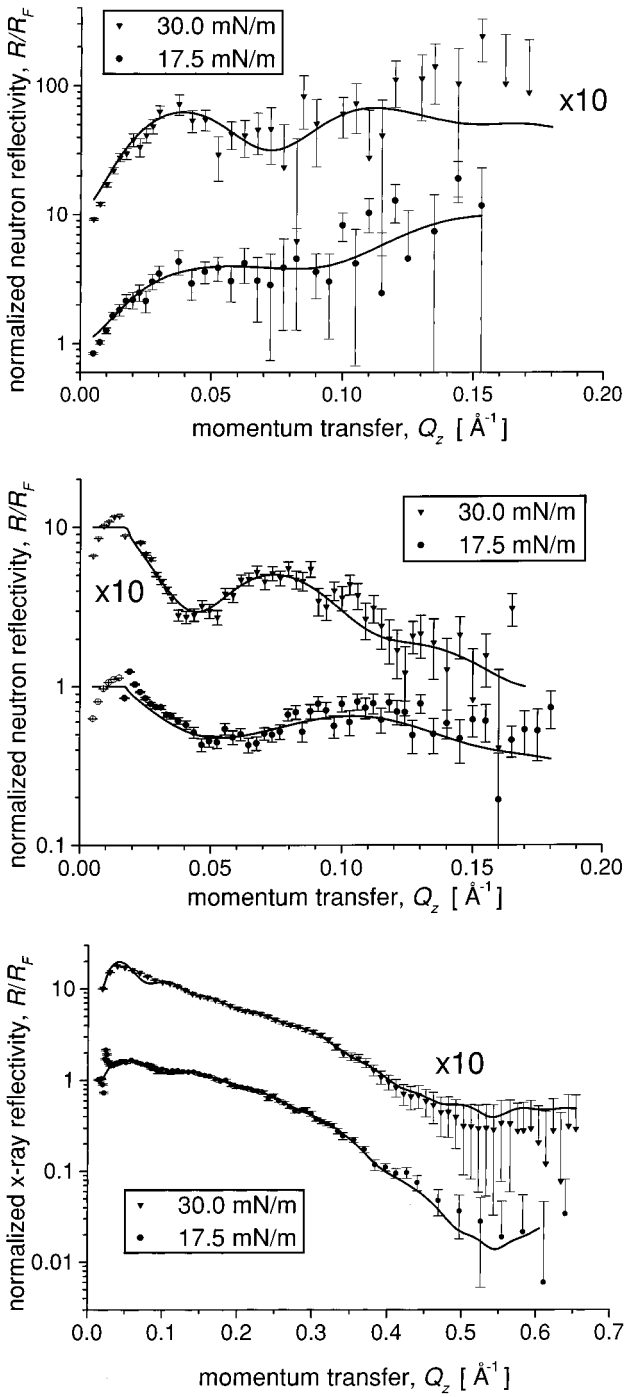

Figure 5. Reflectivity of PMO−$(C_{18})_2$ monolayer films. (a, b) Neutron reflectivity on H_2O and D_2O. (c) X-ray reflectivity on H_2O. For clarity, the data for the films at π = 30 mN/m have been multiplied by 10. The continuous lines are reflectivities computed for models refined with all three data sets at a particular lateral pressure π. Data at subcritical momentum transfer values indicated by open symbols in (b) have not been used in the fitting.

Reflectivity. Figure 5 shows experimental reflectivities of PMO(d_8h_{30})−$(C_{18})_2$ monolayers at π = 17.5 and 30.0 mN/m, observed at T = 15 °C with neutrons on H_2O (a) and D_2O (b) and with X-rays (c). Overlaid are the reflectivities calculated from an average of 16 ensemble conformations, obtained from independent runs of the molecular conformation fit, which describe the two neutron data sets and the X-ray data set

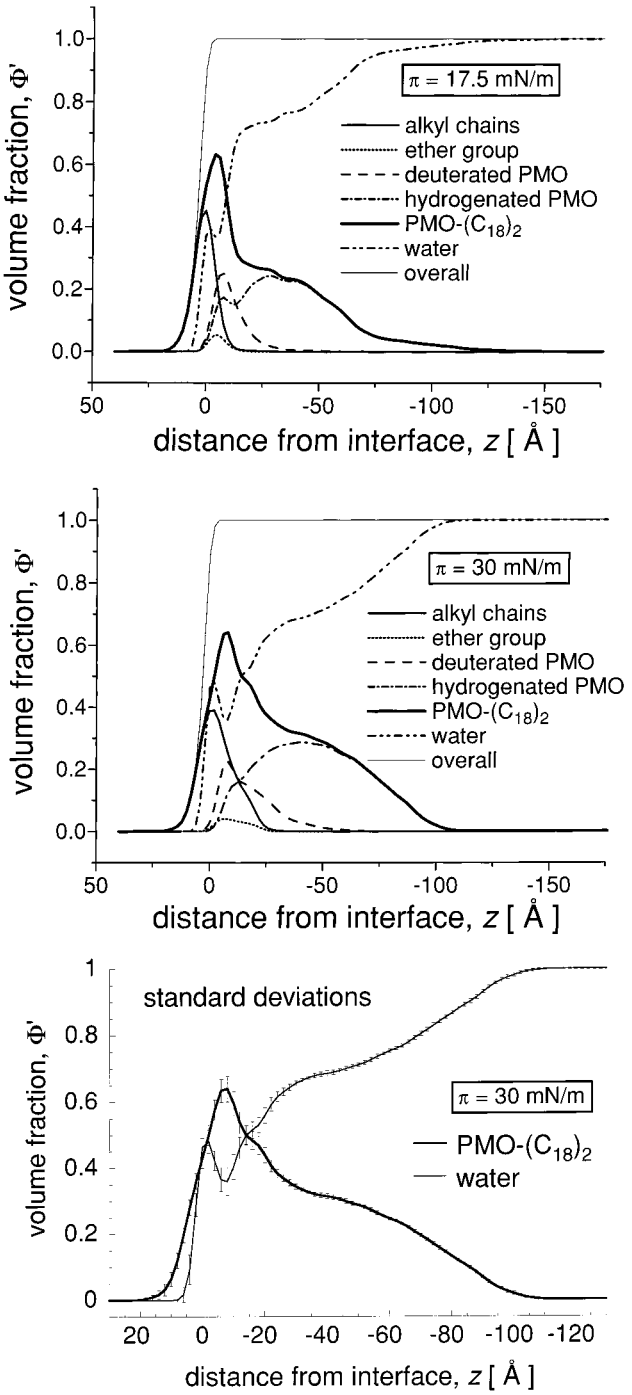

Figure 6. Experimentally determined volume density distributions across the interface derived from the X-ray and neutron scattering length density distributions used to fit the experimental data in Figure 5 simultaneously (sums of 16 independent runs). The organization of the monolayer film is shown (a) below and (b) above the phase transition. (c) Standard deviations of the volume density profile at $\pi = 30$ mN/m.

simultaneously. The corresponding volume density distributions of lipopolymers and water across the interface, $\Phi' = \Phi'(z)$, are shown in Figure 6a for $\pi = 17.5$ mN/m and in Figure 6b for $\pi = 30$ mN/m. The lipopolymer distribution is broken down into contributions from its various constituents: alkyl chains and ether linker group as well as deuterated and hydrogenated PMO chain fragments. The sum of lipopolymer and water volume distributions yields a step function—blurred into an error function with the surface roughness parameter σ—which describes the overall occupation of the space across the interface. At $z > 0$, deviations from the error function envelope occur. The reason is that in the region taken by the hydrophobic chains volume filling is not required, and chain packing defects lead to a somewhat slower decay of the material density toward the air.

Qualitatively, the profiles of the PMO fragment distributions indicate a rather similar molecular organization at both investigated lateral pressures: A sharp maximum (fwhm < 20 Å) of the lipopolymer volume fraction at $z \sim -8$ Å is followed by a plateau that decays gradually, indicative of an extension of the PMO chains to $z \sim -100$ Å. Following the increase in the grafting density upon compression, reflected in the area change from ~190 to ~140 Å^2, the integrated volume density increases accordingly.

From the fragment distributions in Figure 6 it is apparent that the maximum of the lipopolymer density near the interface is not exclusively due to the alkyl chains but contains significant contributions from the PMO chains, both deuterated *and* hydrogenated. Starting from $z = 0$ and going toward the bulk subphase, the water distribution profile mirrors the lipopolymer volume distribution and indicates a steep increase of the water volume fraction near the interface, followed by a narrow dip with a pronounced minimum before the final increase to $\Phi' = 1$ at $z \sim -100$ Å. Clearly, these confined features are at the limit of resolution of the X-ray data and beyond the limit of neutron data sets. However, as revealed from Figure 6c, which displays the standard deviation of Φ' for lipopolymer and water obtained in 16 independent runs, they are not simply an artifact of a particular run: Obviously, the observed extrema in the volume density distributions near the interface are real features of the models.

Major qualitative differences are observed with respect to the organization of hydrophobic alkyl chains and linker fragments along the z axis. Whereas at $\pi = 17.5$ mN/m the alkyl chains are rather closely confined to the interface (fwhm ~ 11 Å), they are spread out further along the surface normal at $\pi = 30$ mN/m (fwhm ~ 19 Å). This is particularly obvious for the anchoring moieties—the ether fragments—which show a broad, almost bimodal distribution at $\pi = 30$ mN/m while they are confined to a narrow region along the surface normal at $\pi = 17.5$ mN/m. Indeed, forced alkyl chain confinement to the interface drastically diminishes the quality of fits to the data, particularly at high π. This suggests strongly that the (partial) immersion of aliphatic chains into the subphase is an important issue for a structural conception of the investigated system in molecular details.

4. Discussion

In what follows we will show that the observed phase transition is due to a polymer-induced condensation of the alkyl chains which is brought about through strain exerted by the PMOs on their lipid anchors. This strain originates from the confinement of the PMOs to the interface which leads to a reduction of their conformational entropy below that of free chains and increases as the surface film is compressed.[31] Across the phase transition, the strain leads to a partial immersion of the alkyl chains into the aqueous subphase which is associated with an increase of their molecular order. We will further show that the polymer brush follows the scaling predictions[11,12] for the segment density along the surface normal generally quite well, although differences occur

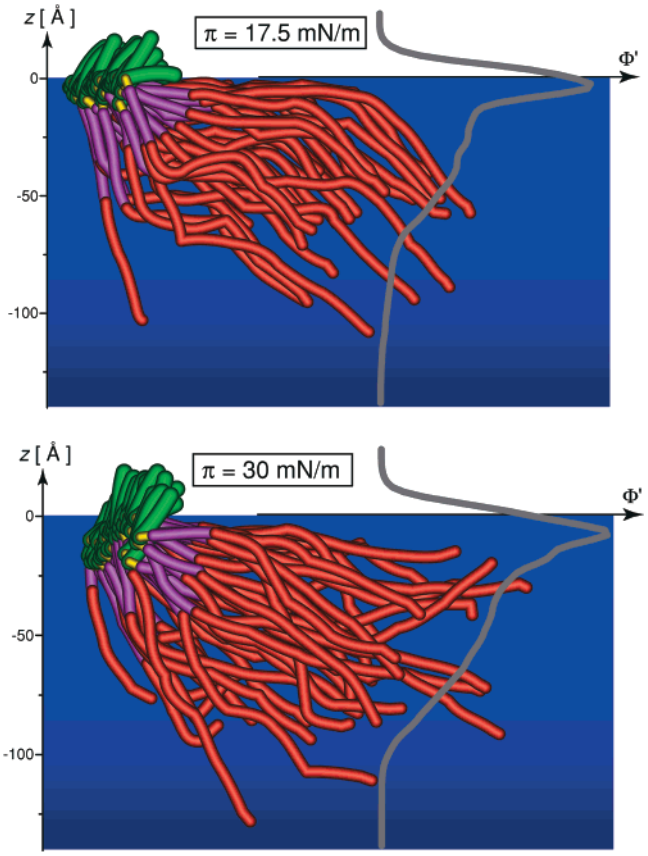

Figure 7. Quasi-molecular rendering of the conformations of an ensemble of 40 molecules representing the lipopolymer monolayer film, as derived from the fitting to the experimental data. Envelope volume density distributions for the lipopolymer ensemble are indicated on the right. Color code: green, alkyl chains (two chains located on one molecule are treated as one cylindrical segment); yellow, ether linker fragment; purple, deuterated PMO fragment; red, hydrogenated PMO fragment.

due to preferential adsorption of the PMO chains to the interface at low surface pressure and the staggered arrangement of the molecules at high surface pressure.

It is easy to demonstrate that the observed phase transitions at $A \sim 150$ Å^2 is not a PMO mushroom-to-brush reorganization: From inserting numbers relevant to the polyoxazoline studied in this work we deduce $r_F = aN^{3/5} \sim 30$ Å. One may thus immediately rule out a mushroom-to-brush transition of the polymer. On the other hand, chain condensation induced by van der Waals interactions, as observed for conventional lipids, may also be ruled out since such transitions occur normally at considerably higher molecular densities, corresponding to $A \sim 70$ Å^2.[14]

Figure 7 illustrates representative molecular conformations of lipopolymer ensembles consistent with the experimental data; 16 such configuration sets were used to derive the molecular density distributions shown in Figure 6. Because of the cylinder symmetry of the problem—reflectivity experiments contain only information on the material density distribution *normal* to the interface—the true three-dimensional conformation is inaccessible. Data analysis, consequently, can only reveal whether a particular subsegment in a chain is more likely to be extended toward the bulk subphase or more parallel to the interface. The ES determines ensemble configurations that fit this overall picture particularly well.

A representation of the ensemble conformations is shown in the upper and lower panels of Figure 7 for the models pertaining to $\pi = 17.5$ mN/m and $\pi = 30$ mN/m, respectively. In this representation, horizontal displacements of a chain are always depicted to occur to the right-hand side, such that the chains within an ensemble that are preferentially oriented in the horizontal direction are visually separated from chains that are preferentially oriented in the normal direction. The strings of subsegments on the molecules are displayed as Bezier curves. Hydrophobic alkyl chains are shown in green, ether linker groups in yellow, deuterated PMO sections in purple, and hydrogenated PMO sections in red. Envelope volume density distributions of the lipopolymer ensemble are indicated on the right. A comparison of the ensemble configurations with the volume density distributions suggests that the waviness of the distributions, most pronounced in the range -30 Å $> z > -80$ Å, is due to the limited ensemble size. In distinction, the pronounced maximum in the lipopolymer volume density near the interface ($z \sim -8$ Å) is a real feature of the model: A number of subfragments are oriented almost horizontal at both pressures. As such a behavior is entropically unfavorable, this implies that attraction between the PMO monomers, probably involving their methyl side groups, and the hydrophobic chains leads to preferential alignment of the polymer with the surface.

A major difference in the organization of the anchoring groups—both the alkyl chains and the ether linkers—at the two lateral pressure values is illustrated in Figure 7. The overall alkyl chain order is higher at $\pi = 30$ mN/m than at 17.5 mN/m. In contrast, the alkyl chains are confined more to the interface at the *lower* surface pressure. A similar molecular organization was observed in reflectivity measurements performed on PEG lipopolymers and evaluated in a more conventional way.[32]

The PMO chain organization is nearly the same at both surface pressures. Whereas the deuterated PMO fragments are slightly better aligned with the surface normal at high π, no difference is detected for the hydrogenated PMO fragments. This is best revealed in Figure 8a, in which the order parameter profiles[21] of both the alkyl and PMO chain fragments at the two explored surface pressures are compared. The order parameter S_{chain}—computed from the molecular organization of 16 representative ensemble conformations in analogy to NMR order parameters[33]—is plotted as a function of the location, l, along the contour line of the lipopolymers. Negative values of l correspond to alkyl chains. Because of the multitude of possible molecular conformations, the standard deviation of the order parameters obtained from 640 molecules (16 independent runs involving 40 molecules) is large. This allows only retrieval of tendencies in the ordering process. Nevertheless, a significant difference in the order parameters is revealed for the alkyl chains and the first section of the PMO chains: Both are more ordered at high π than at low π. Further out on the PMO, the chain order increases at $\pi = 17.5$ mN/m to yield similar values of the order parameter as at $\pi = 30$ mN/m.

In a similar vein, Figure 8b shows the mean distance $\langle d \rangle$ as a function of l. $\langle d \rangle$ has larger values for all l at $\pi = 30$ mN/m than at 17.5 mN/m, due to deeper immersion of the alkyl chains into the aqueous compartment at the higher pressure (up to $l \sim -16$ Å at 30 mN/m as compared with $l \sim -8$ Å at 17.5 mN/m). At the same

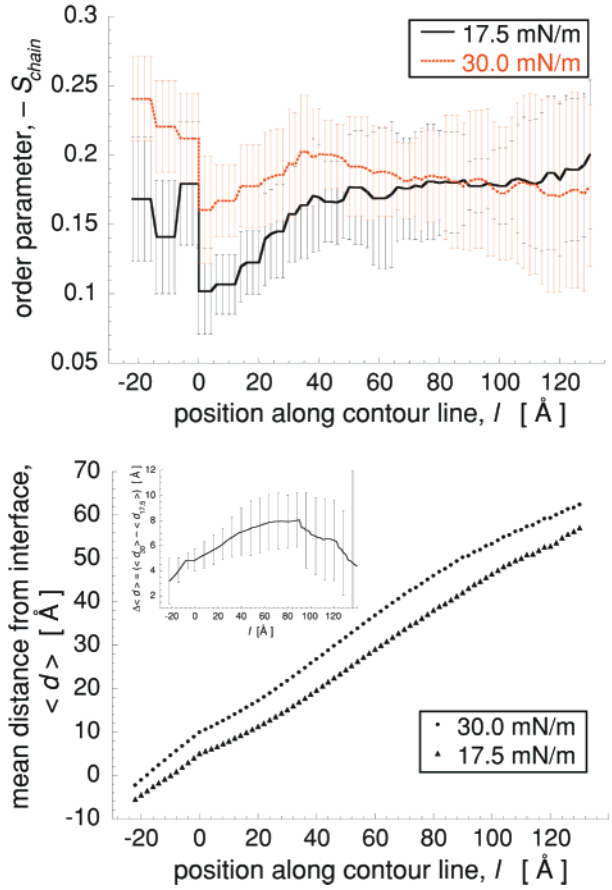

Figure 8. (a, top) Chain order parameters, S_{chain}, and (b, bottom) mean distances, $\langle d \rangle$, from the interface of chain sections of the lipopolymers located at a distance l along their contour lines, as derived from the quasi-molecular representation indicated in Figure 7. The chainlike representation has been divided into sections of $\Delta l = 2$ Å length. $l = 0$ corresponds to the interface between the ether fragment and the alkyl chains, and $l < 0$ indicates sections on the alkyl chains. The inset in (b) shows mean distance differences in films at the two different pressures. Error bars indicate standard deviations within the ensembles. For more details, see text.

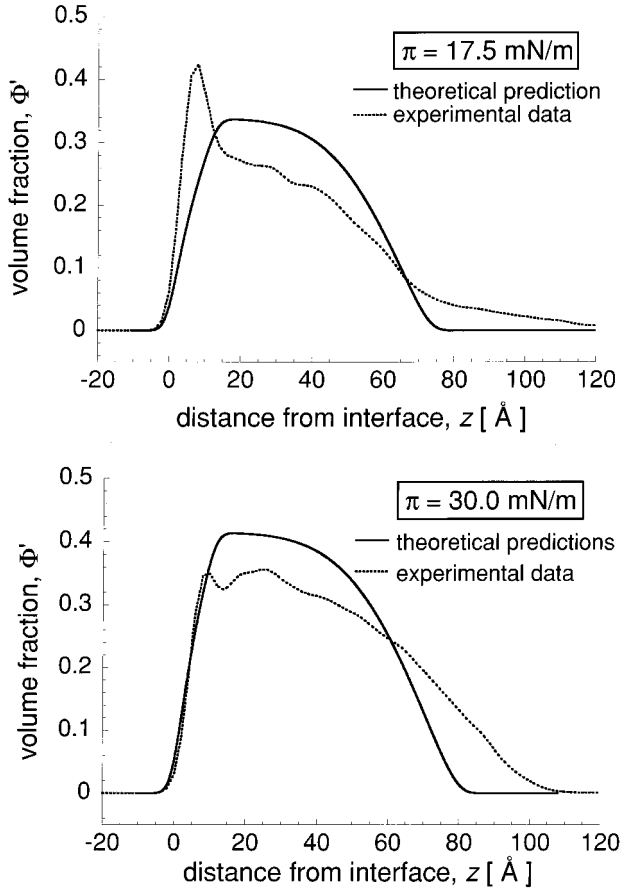

Figure 9. Comparison of the volume density distributions of the lipopolymers' PMO chains (hydrogenated *and* protonated) across the interface at the two different pressures as predicted by theory and determined in the experiments. For details, see text.

time, the slope of the curve at $l < 0$ is larger for $\pi = 30$ mN/m, which implies that the alkyl chains are on average more extended while being submersed. The two traces increase almost in parallel at $l > 0$. A plot of the differences, $\Delta\langle d \rangle = \langle d_{30} \rangle - \langle d_{17.5} \rangle$ (inset in Figure 8b), between the mean distances of corresponding polymer sections at the two pressures shows this more quantitatively. $\Delta\langle d \rangle$ is always positive. It increases slightly at the upper end of the molecules within the ensembles, approximately in the range of -20 Å $< l <$ 40 Å, due to a higher order of the corresponding lipopolymer sections at the higher pressure. Beyond that, $\Delta\langle d \rangle$ is essentially constant. This behavior of $\Delta\langle d \rangle$ implies that a short section of the alkyl chains, already immersed into the subphase at $\pi = 17.5$ mN/m and therefore of higher order than the remaining alkyl subsegments (see Figure 8a), just moves deeper into the subphase without changing conformation across the phase transition. $\Delta\langle d \rangle = 5$ Å is the mean displacement of the molecules toward the subphase. The observation of a slight increase of $\Delta\langle d \rangle$ up to $l \sim 40$ Å implies that the PMO chain subsegments near the interface are stretched by the increasing lateral pressure. At $z \sim 40$ Å and beyond, the stretching levels off, implying that the polymer conformation far from the interface is independent of the lateral pressure in the monolayer.

To apply to the system investigated here theoretical predictions of Alexander and de Gennes, as briefly summarized in section 2, some conditions have to be fulfilled. First, the solvent must be athermal. This condition is met in our experiment since the water solubility of methyloxazoline is high; the pressure/area isotherms at different temperatures also do not show any structural changes; cf. Figure 3. (As is expected for a regular temperature dependence, the plateau simply shifts upon increasing T to higher lateral pressures and smaller areas.) Second, the polymer ought to be uncharged. The observed pH dependence of the isotherms suggests strongly that this is the case. According to theoretical prediction, the PMO chains are thus in a brushlike conformation. Our experimental findings are in accordance with this assignment (cf. Figure 9): No distinctive change in the polymer volume density profile across the phase transition is observed. To enable a more quantitative comparison between theory and experimental results, we have computed the area density of polymer segments, $\Sigma(z)$, and thus their volume density profile, $\Phi'(z)$, according to the scaling concept, taking into account the length distribution of the polymer. Close to the interface ($z < D$), $\Phi = \Sigma(z = 0)(z/a)^{2/3}$; cf. eq 4.

$$n_{if} = \frac{3}{5}\left(\frac{D}{a}\right)^{5/3} \tag{6}$$

A number of monomers are located within this region of the polymer layer. Thus, only $N' = N - n_{if}$ monomers

form the brush with a nonuniform density due to the length distribution of the polymer. If ξ denotes the position along the contour line of a polymer chain ($d\xi = a dN'$), we may write

$$dL(\xi) = \Sigma(\xi)^{1/3}\, d\xi \tag{7}$$

If Σ is assumed to be distributed according to an error function

$$\Sigma(\xi) = \frac{1}{2}\left(1 - \mathrm{erf}\left(\frac{\xi - \xi_m}{\sqrt{2}\kappa}\right)\right) \tag{8}$$

$\Sigma(z)$ is then given by the implicit form ($z(\xi)$, $\Sigma(\xi)$). In Figure 9, the function is plotted for the two surface pressures together with the experimental results, after conversion into volume fraction Φ', and convolution with a Gaussian function, which mimics the influence of capillary waves. For the low surface pressure regime, the interfacial regimes of such profiles agree quite well, although at a distance of a few angstroms from the interface, significant deviations are obvious: Instead of the predicted transition into a flat profile, an accumulation of polymer is experimentally observed close to the interface.

For an ideal hydrophilic polymer, interfacial adsorption is supposed to be weak. The experimental results show that the interaction of PMO with the interface must be taken into account at low pressure (Figure 9, top). Decreasing the area forces the surface-adsorbed PMO moieties to extend deeper into the subphase; adsorption is then less pronounced. Comparison of experimental and theoretical profiles becomes thus more salient in the high-pressure region (Figure 9, bottom). The remaining differences in the slopes are largely due to immersion of the alkyl moieties into the aqueous subphase. In the theory, polymer chain ends are strictly confined to interfaces. Our experimental results show, however, that at $\pi = 30$ mN/m the hydrophobic anchors of the lipopolymers may penetrate into the aqueous subphase by as much as 20 Å. This leads to the slower rise of the polymer volume fraction near the interface and also diminishes the decay toward the subphase. However, the general conclusion from the present analysis is that the observed polymer density distribution follows quite well the expected distribution of a polymer brush at the two respective grafting densities.

We suggest that the phase transition observed in the isotherm shown in Figures 2 and 3, and also hinted at in FT-IRRAS measurements,[6,13] is a polymer-induced alkyl chain condensation accompanied by a reorganization of the chains into a staggered arrangement. At pressures below the transition, the alkyl chains in the lipopolymers are disordered, while the lipid moieties are confined to the interface. The grafted PMO chains thus exert a strain on their lipid anchors: Confined to one half-space, they are incapable of conformationally exploring the other half-space which lowers their configurational entropy.[31] At low pressures, an intimate entwinement of the disordered alkyl chains prevents their (partial) immersion into a subphase. However, as the molecular area decreases upon compression, not only the lateral pressure but also the normal strain increases. This leads to a polymer-induced ordering of the lipid that relieves this strain by staggering the alkyl chains. Such an ordering is expected to result in a lowering of the methylene chain vibration frequencies[34] which has been indeed observed in IR measurements.[13] Immersion of the chains into the subphase has also been observed in X-ray reflectivity and GIXD measurements on lipid-anchored PEG's,[35,36] so that one may infer that this behavior is generic for lipopolymers at surfaces.

5. Conclusions

We have investigated the lipopolymer PMO−$(C_{18})_2$ by complementary neutron and X-ray reflectivity measurements. Despite the limitation of experiments due to low intensity or contrast, the application of a quasi-molecular conformational analysis of ensemble configurations of the lipopolymers at the air/water interface and the coupling of corresponding data sets in a composition-refinement approach yields a detailed conception of the surface structure. Distinctive from theoretical predictions for the brush regime,[11,12] the experimentally determined ensemble conformations show an increased density of the PMO moiety near the interface, indicative of attractive interaction between the hydrophilic polymer and the hydrophobic half-space. This aggregation, probably caused by attraction between PMO and the alkyl chains, might be of importance with regard to applications of PMO in the context of surface modification in general and for the sterical stabilization of vesicles in particular.

Upon compression, the strain which the polymer chains exert on their lipid anchors—and which originates from a reduction of the conformational entropy due to their confinement to the interface[31]—increases. This in turn causes an alkyl chain transition that leads concurrently to a condensation and a staggering of the chains. The experimentally observed phase transition is thus interpreted as a polymer-induced ordering process of the alkyl chains brought about by their partial immersion into the subphase. This interpretation is in accordance with the conclusions from IRRAS studies, that the transition is "native" to the lipopolymer, in the sense that both parts of the molecule are required for its appearance,[6] which suggests that the phase transition is generic for lipopolymers.

Acknowledgment. We thank T. Gutberlet for assistance with the reflectivity measurements and O. Oliveira for thoughtfully reading the manuscript. This work was financially supported by the Deutsche Forschungsgemeinschaft (SFB 294, TP G10; SFB 266, TP C8), the Fonds der Chemischen Industrie, Frankfurt/M., and the EU (TMR Contract ERBFMGECT950059).

Note Added in Proof. In a recent paper (Ahrens et al., *Chem. Phys. Chem.* **2000**, *2*, 101), the structure of lipopolymer monolayers has been characterized on aqueous and solid surfaces with techniques that partially complement our methods. In that case, lateral phase separation of the system on the nanometer length scale has been inferred by the authors. While we are unable to detect such phase separation with the techniques employed in our study, we note that our conclusions are consistent with those drawn in this earlier study as far as the molecular organization *normal to the surface* is concerned.

References and Notes

(1) Lasic, D.; Martin, D. *Stealth Liposomes*; CRC Press: Boca Raton, FL, 1995.
(2) Blume, G.; Cevc, C. *Biochim. Biophys. Acta* **1990**, *1029*, 91−97.

(3) Zalipsky, S.; Hansen, C. B.; Oaks, J. M.; Allen, T. M. *J. Pharm. Sci.* **1996**, *85*, 133−137.
(4) Frey, W.; Schneider, J.; Ringsdorf, H.; Sackmann, E. *Macromolecules* **1987**, *20*, 1312−1321.
(5) Lasic, D. D.; Needham, D. *Chem. Rev.* **1995**, *95*, 2601−2628.
(6) Baekmark, T. R.; Wiesenthal, T.; Kuhn, P.; Albersdörfer, A.; Nuyken, O.; Merkel, R. *Langmuir* **1999**, *15*, 3616−3626.
(7) Zalipsky, S. *Adv. Drug Delivery Rev.* **1995**, *16*, 157−182.
(8) Woodle, D. R.; Lasic, D. D. *Biochim. Biophys. Acta* **1992**, *1113*, 171−199.
(9) Beugin, S.; Edwards, K.; Karlsson, G.; Ollivon, M.; Lesieur, S. *Biophys. J.* **1998**, *74*, 3198−3210.
(10) Kuhn, P.; Weberskirch, R.; Nuyken, O.; Cevc, G. *Des. Monomers Polym.* **1998**, *1*, 327−346.
(11) Alexander, S. *J. Phys. (Paris)* **1977**, *38*, 983−987.
(12) de Gennes, P. G. *Adv. Colloid Interface Sci.* **1987**, *27*, 189−209.
(13) Baekmark, T. R.; Wiesenthal, T.; Kuhn, P.; Bayerl, T. M.; Nuyken, O.; Merkel, R. *Langmuir* **1997**, *13*, 5521−5523.
(14) Albrecht, O.; Gruler, H.; Sackmann, E. *J. Phys. (Paris)* **1978**, *39*, 301−313.
(15) Wiesenthal, T.; Baekmark, T. R.; Merkel, R. *Langmuir* **1999**, *15*, 6837−6844.
(16) Wurlitzer, A.; Politsch, E.; Cevc, G.; Gutberlet, T.; Kjaer, K.; Lösche, M. *Physica B* **2000**, *276−278*, 343−344.
(17) Wilhelmy, L. *Ann. Phys.* **1863**, *119*, 177−217.
(18) Krüger, P.; Schalke, M.; Linderholm, J.; Lösche, M. *Rev. Sci. Instrum.* **2001**, *72*, 184−192.
(19) TAS9 (for technical specifications, see ACS Electronic Supporting Information) was the MARK-2 implementation following the MARK-1 reflectometer at TAS7 (cf.: Vaknin, D.; Kjær, K.; Als-Nielsen, J.; Lösche, M. A new liquid surface neutron reflectometer and its application to the study of DPPC in a monolayer at the air/water interface. *Makromol. Chem. Macromol. Symp.* **1991**, *46*, 383−388). With the recent permanent shutdown of DR3, TAS9 is regrettably no longer available.
(20) Schwefel, H.-P. *Evolution and Optimum Seeking*; J. Wiley & Sons: New York, 1995.
(21) Politsch, E.; Cevc, G.; Wurlitzer, A.; Lösche, M. *Macromolecules* **2001**, *34*, 1328.
(22) Helm, C. A.; Möhwald, H.; Kjaer, K.; Als-Nielsen, J. *Europhys. Lett.* **1987**, *4*, 697−703.
(23) Bosio, L.; Benattar, J. J.; Rieutord, F. *Rev. Phys. Appl.* **1987**, *22*, 775−778.
(24) Armen, R. S.; Uitto, O. D.; Feller, S. E. *Biophys. J.* **1998**, *75*, 734−744.
(25) Connolly, M. L. *Appl. Crystallogr.* **1983**, *16*, 548−558.
(26) Wiener, M. C.; White, S. H. *Biophys. J.* **1991**, *59*, 174−185.
(27) Vaknin, D.; Kjaer, K.; Als-Nielsen, J.; Lösche, M. *Biophys. J.* **1991**, *59*, 1325−1332.
(28) Rechenberg, I. *Evolutionsstrategie '94*; Frommann-Holzboog: Stuttgart, 1994.
(29) Flory, P. *Principles of Polymer Chemistry*; Cornell University Press: Ithaca, NY, 1971.
(30) de Gennes, P. G. *Macromolecules* **1980**, *13*, 1069−1075.
(31) Hiergeist, C.; Lipowsky, R. *J. Phys. II* **1996**, *6*, 1465−1481.
(32) Kuhl, T. L.; Majewski, J.; Wong, J. Y.; Steinberg, S.; Leckband, D. E.; Israelachvili, J. N.; Smith, G. S. *Biophys. J.* **1998**, *75*, 2352−2362.
(33) Egberts, E.; Marrink, S.-J.; Berendsen, H. J. C. *Europ. Biophys. J.* **1994**, *22*, 423−436.
(34) Mendelsohn, R.; Brauner, J. W.; Gericke, A. *Annu. Rev. Phys. Chem.* **1995**, *46*, 305−334.
(35) Majewski, J.; Kuhl, T. L.; Gerstenberg, M. C.; Israelachvili, J. N.; Smith, G. S. *J. Phys. Chem. B* **1997**, *101*, 3122−3129.
(36) Kuhl, T. L.; Majewski, J.; Howes, P. B.; Kjaer, K.; von Nahmen, A.; Lee, K. Y. C.; Ocko, B.; Israelachvili, J. N.; Smith, G. S. *J. Am. Chem. Soc.* **1999**, *121*, 7682−7688.

MA000932N